Journal of Power Sources 195 (2010) 5057–5061

Contents lists available at ScienceDirect

Journal of Power Sources

journal homepage: www.elsevier.com/locate/jpowsour

Short communication

Synthesis and electrochemical performances of $Li_3V_2(PO_4)_3$/(Ag + C) composite cathode

L. Zhang, X.L. Wang, J.Y. Xiang, Y. Zhou, S.J. Shi, J.P. Tu*

State Key Laboratory of Silicon Materials and Department of Materials Science and Engineering, Zhejiang University, Hangzhou 310027, China

ARTICLE INFO

Article history:
Received 21 August 2009
Received in revised form 8 February 2010
Accepted 8 February 2010
Available online 12 February 2010

Keywords:
Lithium vanadium phosphate
Composite
Cathode
Lithium ion battery

ABSTRACT

$Li_3V_2(PO_4)_3$, $Li_3V_2(PO_4)_3$/C and $Li_3V_2(PO_4)_3$/(Ag + C) composites as cathodes for Li ion batteries are synthesized by carbon-thermal reduction (CTR) method and chemical plating reactions. The microstructure and morphology of the compounds are characterized by X-ray diffraction (XRD), scanning electron microscopy (SEM) and transmission electron microscopy (TEM). The $Li_3V_2(PO_4)_3$/(Ag + C) particles are 0.5–1 μm in diameters. As compared to $Li_3V_2(PO_4)_3$, $Li_3V_2(PO_4)_3$/C, the $Li_3V_2(PO_4)_3$/(Ag + C) composite cathode exhibits high discharge capacity, good cycle performance (140.5 mAh g^{-1} at 50th cycle at 1 C, 97.3% of initial discharge capacity) and rate behavior (120.5 mAh g^{-1} for initial discharge at 5 C) for the fully delithiated (3.0–4.8 V) state. Electrochemical impedance spectroscopy (EIS) measurements show that the carbon and silver co-modification decreases the charge transfer resistance of $Li_3V_2(PO_4)_3$/(Ag + C) cathode, and improves the conductivity and boosts the electrochemical performance of the electrode.

1. Introduction

Since Padhi et al. [1] reported lithium iron phosphate as a cathode material for lithium-ion batteries, transition metal polyanion materials based on PO_4^{3-}, such as $LiMPO_4$ (M = Fe, Mn, Co), $Li_3M'_2(PO_4)_3$ (M′ = Fe, V) and $LiVPO_4F$ have attracted considerable attention and studies as perspective intercalation materials for lithium-ion batteries [2–7]. Among these materials, monoclinic $Li_3V_2(PO_4)_3$ is a highly promising material proposed as cathode for higher voltage lithium-ion batteries because it possesses good ion mobility, highest theoretical capacity (197 mAh g^{-1}), high operate voltage (average potential of 3.85 V vs. Li/Li^+), good thermal stability [8–12], and high specific energy density of 2330 mWh cm^{-3} comparable to $LiFePO_4$ (2065 mWh cm^{-3}) [13].

Usually, monoclinic $Li_3V_2(PO_4)_3$ materials are obtained through high temperature solid-state reactions [3–5,12,14–20] or sol–gel methods followed by heat treatment [21–23]. However, the low electronic conductivity of $Li_3V_2(PO_4)_3$ leads to poor electrode conductivity and cycling performance [11,24]. Therefore many researches had been devoted to solving this problem, such as coating with carbon [8,20,25–28] and doping other metals (Fe, Cr, Al, Y, etc.) [17,29] to $Li_3V_2(PO_4)_3$. But large amount of electrochemically inactive carbon (10–15 wt.%) will decrease the volumetric energy density of electrodes severely. Therefore, the amount of carbon in $Li_3V_2(PO_4)_3$/C composite would be minimized, and some electronic conductive Ag coating could be effective to achieve better electrochemical performance but not sacrifice the specific energy density.

In the present work, we synthesized $Li_3V_2(PO_4)_3$/(Ag + C) composite by carbon-thermal reduction (CTR) method and chemical plating reactions. Polypropylene (PP) was used as both reduction agent and carbon source. The morphology modification mechanism under the effect of Ag and C co-modification is discussed and the improved electrochemical performances of $Li_3V_2(PO_4)_3$/(Ag + C) composite as the cathode active material are investigated.

2. Experimental

Stoichiometric Li_2CO_3, $NH_4H_2PO_4$ and NH_4VO_3 were dispersed in alcohol and ball milled in a planetary mill for 10 h. The mass rate of ball to powder was 10:1 and the rotation speed was 350 rpm. After alcohol was evaporated, the precursor was firstly decomposed at 350 °C for 4 h. Then, the resulting powder was reground and transferred to a tube furnace, sintered at 900 °C for 8 h in Ar flow to get pure $Li_3V_2(PO_4)_3$. The $Li_3V_2(PO_4)_3$/C composites with about 4.0% carbon in weight were prepared using polypropylene (PP) as both reduction agent and carbon source, which was added to the same raw materials as that for the preparation of $Li_3V_2(PO_4)_3$. The $Li_3V_2(PO_4)_3$/(Ag + C) composite was prepared by adding the as-prepared $Li_3V_2(PO_4)_3$/C particles into a mixed solution of 0.03 M $AgNO_3$ and 0.03 M glucose with stirring for 2 h. The precipitates were separated by centrifugation, washed with deionized water and ethanol for several times, and dried in vacuum at 110 °C for 12 h.

* Corresponding author. Tel.: +86 571 8795 2573; fax: +86 571 8795 2856.
E-mail addresses: wangxl@zju.edu.cn (X.L. Wang), tujp@zju.edu.cn (J.P. Tu).

0378-7753/$ – see front matter © 2010 Elsevier B.V. All rights reserved.
doi:10.1016/j.jpowsour.2010.02.014

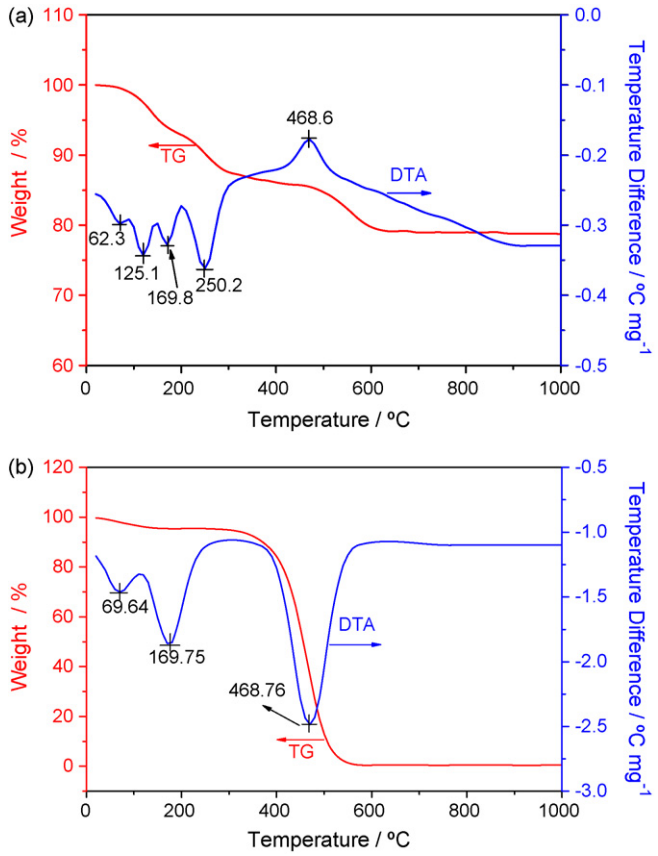

Fig. 1. TG–DTA patterns of the precursor mixture of (a) LVP/C compound and (b) polypropylene power in argon atmosphere.

TG–DTA analysis of the precursor after ball-milling was investigated on a SDT Q600 TG–DTA apparatus at the temperature range from 25 °C to 1000 °C under argon flow with a heating rate of 10 °C min^{-1}. The structures and compositions of $Li_3V_2(PO_4)_3$, $Li_3V_2(PO_4)_3$/C, and $Li_3V_2(PO_4)_3$/(Ag + C) were analyzed by X-ray diffraction (XRD, Philips PC-APD with Cu Kα radiation) and energy-dispersive spectrum (EDS GENENIS 4000), respectively. The morphologies of these compounds were characterized by field emission scanning electron microscopy (FESEM, FEI SIRION) and high-resolution transmission electron microscopy (HRTEM, JEOL JEM-2010F), respectively. Electrical conductivity measurements were carried on CON510, the powders were hot-pressed respectively in a graphite die for 1 h with T = 700 °C, P = 80 MPa in a vacuum uni-axial compressor.

Coin-type cells (CR 2025) were assembled in an argon-filled glove box. The cathode consisted of 80 wt.% as-prepared particles, 10 wt.% acetylene black and 10 wt.% polyvinylidene fluoride (PVDF) on aluminum foil. The anode was metallic lithium foil. 1 M $LiPF_6$ in ethylene carbonate (EC)–dimethyl carbonate (DME) (1:1 in volume) as the electrolyte, and a polypropylene microporous film (Cellgard 2300) as the separator. The galvanostatic charge–discharge tests are conducted on LAND battery program-control test system at different current densities in the voltage range of 3.0–4.8 (vs. Li/Li$^+$) at room temperature. For electrochemical impedance spectroscopy (EIS) measurements, the test cells were with the metallic lithium foil as both the reference and counter electrodes. Cyclic voltammetry (CV) and EIS measurements were performed on CHI660C electrochemical workstation.

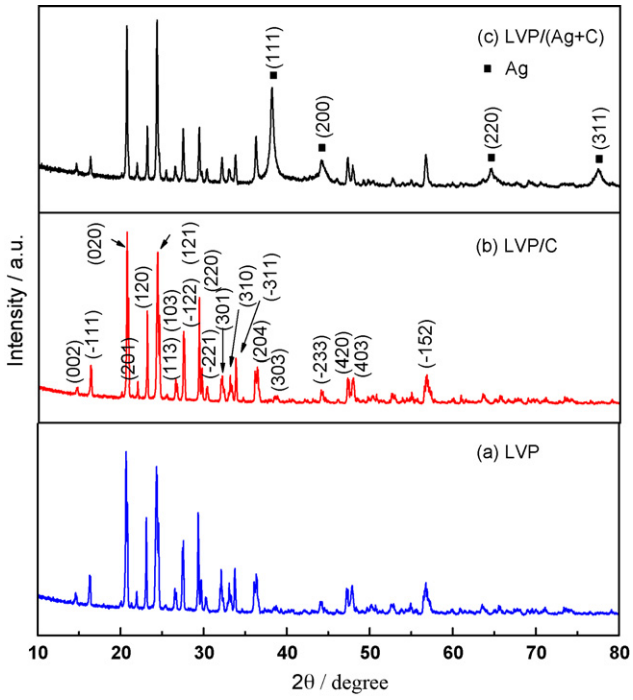

Fig. 2. XRD patterns of (a) $Li_3V_2(PO_4)_3$, (b) $Li_3V_2(PO_4)_3$/C, (c) $Li_3V_2(PO_4)_3$/(Ag + C).

3. Results and discussion

Fig. 1a shows the TG–DTA pattern of the $Li_3V_2(PO_4)_3$/C precursor. The weight loss below 115 °C, from 115 °C to 145 °C, from 145 °C to 220 °C and from 220 °C to 310 °C are attributed to the release of absorbed water, decomposition of constitution water, decomposition of Li_2CO_3, and release of NH_3 from $NH_4H_2PO_4$ and NH_4VO_3, respectively. These processes correspond well with the endothermic peaks in the DTA curve, which locate near 62 °C, 125 °C, 170 °C and 250 °C respectively. The weight loss, which occurs between 400 °C and 600 °C in the TG curve can be ascribed to the formation of $Li_3V_2(PO_4)_3$, and the pyrolysis of polypropylene (PP) around 470 °C. The incline, which distributes between 466 °C and 900 °C in the DTA curve can be ascribed to the crystallization of $Li_3V_2(PO_4)_3$. Thermal behavior of polypropylene in Ar atmosphere is shown in Fig. 1b. There are two plateaus for weight loss in TG curve from 20 °C to 1000 °C, while there are three endothermic peaks in the corresponding DTA curve, at about 70 °C, 170 °C, and 470 °C, respectively. The first small peak at 70 °C is related to the loss of physical water. The second one at 170 °C corresponds to the melting process of polypropylene. The sharpest peak at 470 °C is attributed to the pyrolysis of polypropylene. Compared to the inflexion temperature in Fig. 1a, the weight loss above 480 °C is insignificant, which is close to the pyrolysis temperature of polypropylene at 470 °C. From the TG–DTA curves, it can be concluded that the reaction stops at 900 °C. According to this result, we choose 900 °C as the sintering temperature. $Li_3V_2(PO_4)_3$/C composite was synthesized by solid state reaction method by the following reactions:

$$4NH_4VO_3 + 3Li_3CO_3 + 6NH_4H_2PO_4 + CH_3(CH_2CH)_n \rightarrow 2Li_3V_2(PO_4)_3 + 4CO_2 + 10NH_3 + 13H_2O + 2nC + \frac{3n+1}{2H_2} \quad (1)$$

Fig. 2 shows the XRD patterns of the as-prepared samples. As shown in pattern a, all the sharp diffraction peaks correspond well with monoclinic $Li_3V_2(PO_4)_3$ (space group $P2_1/n$(14), JCPDS 47-0107). The structure of $Li_3V_2(PO_4)_3$ in $Li_3V_2(PO_4)_3$/C composite does not change and still exhibits typical monoclinic system (pat-

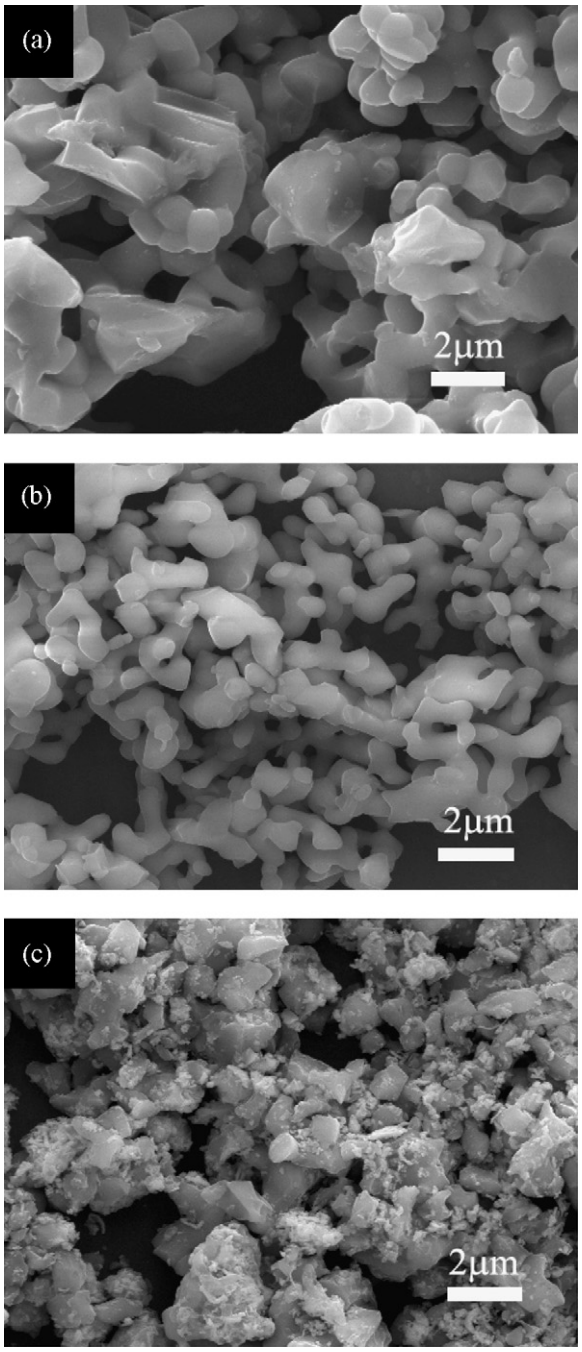

Fig. 3. SEM images (a) $Li_3V_2(PO_4)_3$, (b) $Li_3V_2(PO_4)_3$/C, (c) $Li_3V_2(PO_4)_3$/(Ag + C).

tern b). For the $Li_3V_2(PO_4)_3$/(Ag + C) composite (pattern c), except for the diffraction peaks of $Li_3V_2(PO_4)_3$, the peaks locate at 38.08°, 44.05°, 64.53° and 77.33° can be assigned to (1 1 1), (2 0 0), (2 2 0) and (3 1 1) crystal faces of Ag (*Fm*-3*m*(225), JCPDS 65-2871). The existence of carbon and silver in the composite was also identified by EDS. The $Li_3V_2(PO_4)_3$/(Ag + C) composite synthesized in this work contains 3.8 wt.% C and 5.1 wt.% Ag determined by the EDS analysis.

SEM images of $Li_3V_2(PO_4)_3$, $Li_3V_2(PO_4)_3$/C and $Li_3V_2(PO_4)_3$/(Ag + C) composite are shown in Fig. 3. The pure $Li_3V_2(PO_4)_3$ particles are about 1–3 μm in diameter and agglomerate extensively with each other as shown in Fig. 3a. The size of $Li_3V_2(PO_4)_3$/C particles are smaller and more uniform than pure $Li_3V_2(PO_4)_3$ with diameters of 0.5–1.0 μm, as presented in Fig. 3b. The smooth surface of the particles indicates that the carbon layer coated on $Li_3V_2(PO_4)_3$ is thin and homogeneous. As seen in Fig. 3c, the surface of the $Li_3V_2(PO_4)_3$/(Ag + C) composite are not as smooth as $Li_3V_2(PO_4)_3$/C. Tiny Ag nanoparticles disperse uniformly on the surface of $Li_3V_2(PO_4)_3$/C particles, which act as a bridge to connect each $Li_3V_2(PO_4)_3$/C particle to form a coarse structure. This microstructure facilitates the electronic transfer among the $Li_3V_2(PO_4)_3$ particles, which leads to higher capacity and enhances the high rate property of $Li_3V_2(PO_4)_3$/(Ag + C) composite.

HRTEM is used to further investigate the morphology of the as-prepared particles. Fig. 4a and b shows the HRTEM image of pure $Li_3V_2(PO_4)_3$ and $Li_3V_2(PO_4)_3$/C composite, respectively. As compared to the smooth surface of pure $Li_3V_2(PO_4)_3$, the $Li_3V_2(PO_4)_3$/C composite particle is coated with an amorphous carbon layer with about 5 nm in thickness. From the HRTEM images of $Li_3V_2(PO_4)_3$/(Ag + C) in Fig. 4c and d, it can be seen that high dispersed Ag nanoparticles with diameter of about 15 nm are loaded on the $Li_3V_2(PO_4)_3$/C particles. The existence of Ag nanoparticles can also be confirmed in the lattice image under a high magnification (Fig. 4d).

Fig. 5 shows the initial charge–discharge curves of the three electrodes at 0.1 C (1 C = 197 mAh g^{-1}) from 3.0 V to 4.8 V. All the electrodes show the similar charge–discharge behaviors. Four plateaus appear in the charge curves around 3.6 V, 3.8 V, 4.1 V and 4.6 V, which correspond to the phase transformation from $Li_3V_2(PO_4)_3$ to $Li_xV_2(PO_4)_3$, where x = 2.5, 2, 1 and 0, respectively [10]. During the discharging process, there are three plateaus at around 3.6 V, 3.7 V and 4.0 V, corresponding to the reverse processes of the frontal three charge plateaus. But the plateau voltage separations become lower after carbon and silver co-modification. The lower electrochemical polarization suggests the higher conductivity and leads to better electrochemical property [30]. Compared to $Li_3V_2(PO_4)_3$ and $Li_3V_2(PO_4)_3$/C, the charge plateaus of $Li_3V_2(PO_4)_3$/(Ag + C) shifts to a relative high location, the initial discharge specific capacity of $Li_3V_2(PO_4)_3$/(Ag + C) (172.0 mAh g^{-1}) is much higher than that of $Li_3V_2(PO_4)_3$ (141.7 mAh g^{-1}) and $Li_3V_2(PO_4)_3$/C (162.0 mAh g^{-1}). What's more, the initial coulombic efficiency is also improved of the $Li_3V_2(PO_4)_3$/(Ag + C) composite (99%) rather than that of $Li_3V_2(PO_4)_3$ (85%) and $Li_3V_2(PO_4)_3$/C (98%).

The cycling performances of $Li_3V_2(PO_4)_3$, $Li_3V_2(PO_4)_3$/C and $Li_3V_2(PO_4)_3$/(Ag + C) at different current densities are shown in Fig. 6. After 50 cycles, the $Li_3V_2(PO_4)_3$/C and $Li_3V_2(PO_4)_3$/(Ag + C) can sustain 94.3% (148.7 mAh g^{-1}) and 95.0% (162.7 mAh g^{-1}) capacity of the 1st cycle at 0.1 C rate, but the capacity of $Li_3V_2(PO_4)_3$ decreases from 141.2 mAh g^{-1} to 101.7 mAh g^{-1}, only 72% capacity sustains. The high reversible capacity and good coulombic efficiency of $Li_3V_2(PO_4)_3$/(Ag + C) can be attributed to the carbon and silver co-modification. Ag provides high conductivity. It also can be seen from cycle performance at 1 C, the capacity of $Li_3V_2(PO_4)_3$ drops quickly but $Li_3V_2(PO_4)_3$/C and $Li_3V_2(PO_4)_3$/(Ag + C) sustain high capacity. As the current density increases to 5 C, the capacity of $Li_3V_2(PO_4)_3$/C drops quickly, while the $Li_3V_2(PO_4)_3$/(Ag + C) can still maintain 96.3% (120.5 mAh g^{-1}) capacity of the 1st cycle.

The initial CV curves for the $Li_3V_2(PO_4)_3$, $Li_3V_2(PO_4)_3$/C and $Li_3V_2(PO_4)_3$/(Ag + C) electrodes between 3.0 V and 4.8 V at a scan rate of 0.1 mV s^{-1} are presented in Fig. 7. There are four oxidation peaks and three reduction peaks in the curves, which are in great agreement with the charge/discharge plateaus presented in Fig. 5 and some previous publications [11,22,23]. In Fig. 7, though the shape does not change greatly indicating that there is no change in redox behavior in the electrodes, there are some apparent differences among the three curves. First, the peak of current density of the $Li_3V_2(PO_4)_3$/(Ag + C) electrode is higher than that of the $Li_3V_2(PO_4)_3$/C and $Li_3V_2(PO_4)_3$ electrodes. Second, the potential differences between anodic peaks and cathodic peaks are small-

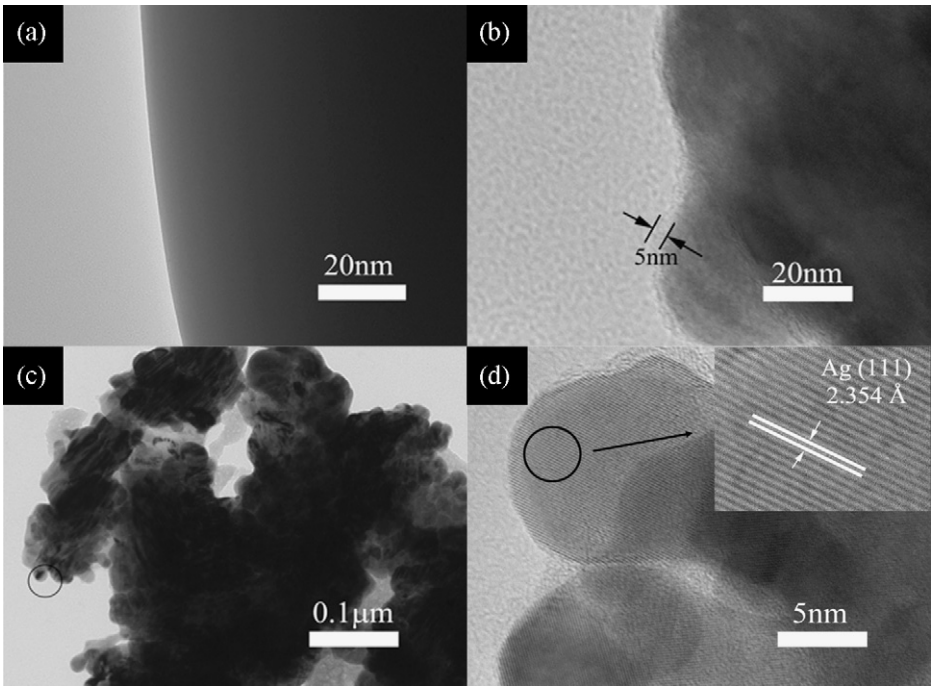

Fig. 4. TEM images of (a) $Li_3V_2(PO_4)_3$, (b) $Li_3V_2(PO_4)_3$/C, (c) $Li_3V_2(PO_4)_3$/(Ag + C) and HRTEM image of (d) $Li_3V_2(PO_4)_3$/(Ag + C).

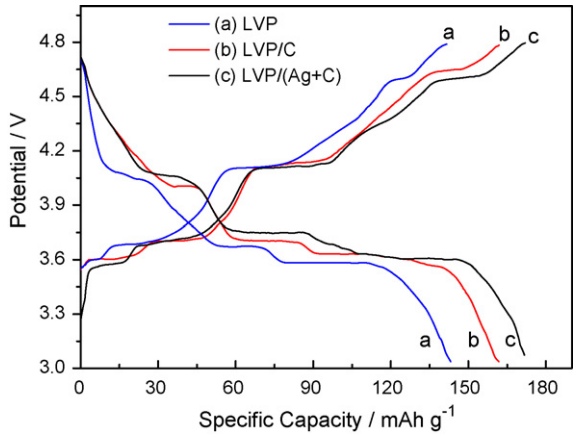

Fig. 5. The first charge/discharge curves for (a) $Li_3V_2(PO_4)_3$, (b) $Li_3V_2(PO_4)_3$/C, (c) $Li_3V_2(PO_4)_3$/(Ag + C) electrodes.

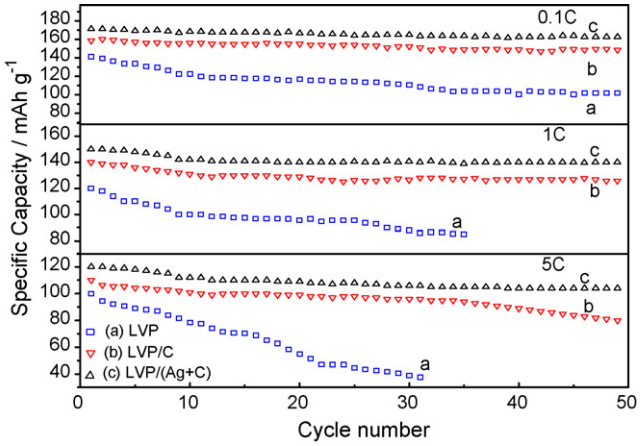

Fig. 6. Cycling performances of (a) $Li_3V_2(PO_4)_3$, (b) $Li_3V_2(PO_4)_3$/C, (c) $Li_3V_2(PO_4)_3$/(Ag + C) electrodes at different current densities.

est for the $Li_3V_2(PO_4)_3$/(Ag + C) electrode, indicating enhancement of the reversibility in the electrode reaction due to the presence of carbon shell and Ag modification in $Li_3V_2(PO_4)_3$/(Ag + C) electrode.

To further understand the electrochemical behaviors of the as-prepared samples, electrochemical impedance spectroscopy measurements were used to study the electrode reaction kinetics of different samples, and they were carried out by applying an AC voltage of 5 mV in the frequency range of 10 mHz to 100 kHz at the discharge state (3.6 V) in the 20th cycles. As shown in Fig. 8a, there are three regions of all three curves, an intercept at high frequency represents the resistance of the electrolyte (R_e) and electrode, a high-middle frequency semicircle represents the charge-transfer process (R_{ct}) and the low frequency region of a inclined line is attributed to the diffusion of the lithium ions into the electrode material (R_b). Fig. 8b presents an equivalent circuit to fit the electrochemical impedance spectroscopy. Constant phase elements CPE_{dl} and CPE_b represent double layer and bulk capacitance. We can see that R_e is similar for all three electrodes, and its value is very low

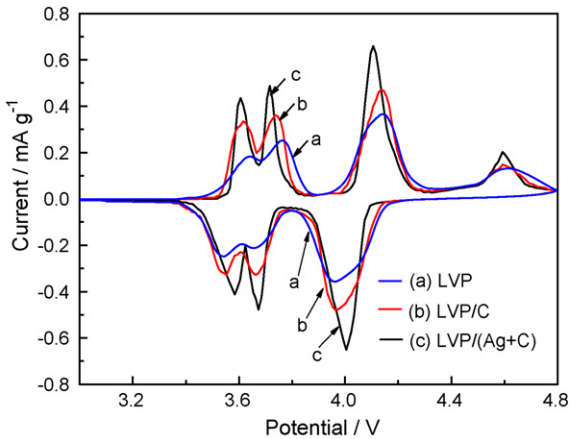

Fig. 7. The cyclic voltammogram curves of (a) $Li_3V_2(PO_4)_3$, (b) $Li_3V_2(PO_4)_3$/C, (c) $Li_3V_2(PO_4)_3$/(Ag + C) electrodes at scan rate of 0.1 mV s^{-1} from 3.0 V to 4.8 V.

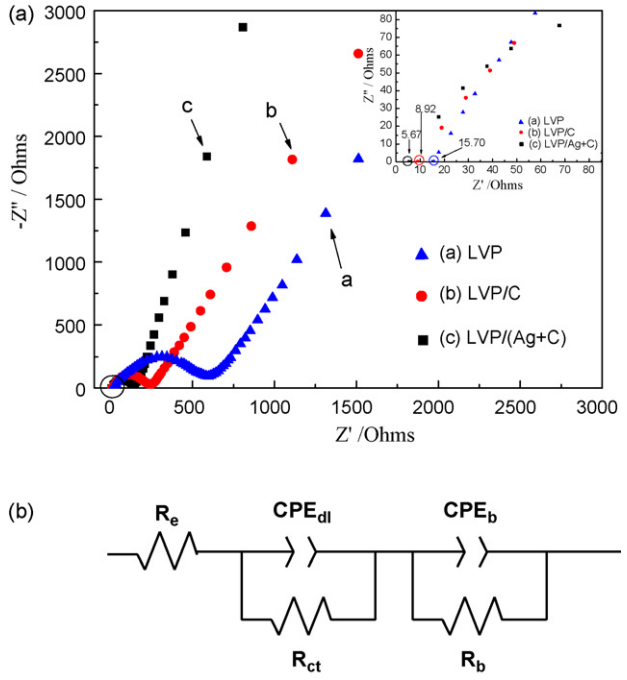

Fig. 8. (a) Impedance spectra of (a) $Li_3V_2(PO_4)_3$, (b) $Li_3V_2(PO_4)_3$/C, (c) $Li_3V_2(PO_4)_3$/(Ag + C) electrodes measured at the discharge potential of 3.6 V in the 20th cycles. (b) Equivalent circuit used for fitting the experimental impedance data.

comparing to R_{ct} and R_b. Calculating the diameter of the semicircle of the three curves, it can be found that $Li_3V_2(PO_4)_3$/(Ag + C) shows lower R_{ct} than $Li_3V_2(PO_4)_3$/C, whose R_{ct} is lower than $Li_3V_2(PO_4)_3$. It indicates that the Ag and C co-modification decreases the value of R_{ct}, which plays a critical role in the electrode reaction kinetics. The electronic conductivity is improved and the insertion/exertion behavior of lithium is enhanced. Electronic conductivity measurement illustrates that the electrical conductivity of $Li_3V_2(PO_4)_3$, $Li_3V_2(PO_4)_3$/C and $Li_3V_2(PO_4)_3$/(Ag + C) are 0.086 S cm^{-1}, 1.49 S cm^{-1} and 13.76 S cm^{-1}, respectively. The electrical conductivity of $Li_3V_2(PO_4)_3$ is apparently increased due to the Ag and C co-modification, which is preferable for the enhancement in electrochemical Li^+ insertion performances of phosphate-based Li^+ intercalation materials. Thus, the utilization degree of $Li_3V_2(PO_4)_3$ is increased by the increase of the electrical conductivity, resulting in the decrease of R_{ct} as mentioned above.

4. Conclusions

$Li_3V_2(PO_4)_3$/(Ag + C) composite is synthesized by carbon-thermal reduction (CTR) method using polypropylene (PP) as both reduction agent and carbon source and chemical plating on $Li_3V_2(PO_4)_3$/C. The carbon and silver co-modification improves the electrode reaction kinetics in terms of discharge capacity and rate capability. The discharge capacity is improved from 162 mAh g^{-1} for $Li_3V_2(PO_4)_3$/C to 172 mAh g^{-1} for $Li_3V_2(PO_4)_3$/(Ag + C), and good cycle performance (140.5 mAh g^{-1} at 50th cycle under 1 C rate, 97.3% of initial discharge capacity) and excellent rate behavior (120.5 mAh g^{-1} under 5 C rate for initial discharge) are obtained. Electrochemical impedance spectroscopy (EIS) measurement shows that the carbon and silver co-modification decreases the charge transfer resistance of $Li_3V_2(PO_4)_3$/(Ag + C) cathode.

References

[1] A.K. Padhi, K.S. Najundaswamy, J.B. Goodenough, J. Electrochem. Soc. 144 (1997) 1188–1194.
[2] S.C. Yin, H. Grondey, P. Strobel, H. Huang, L.F. Nazar, J. Am. Chem. Soc. 125 (2003) 326–327.
[3] D. Morgan, G. Ceder, M.Y. Saidi, J. Swoyer, H. Huang, G. Adamson, Chem. Mater. 14 (2002) 4684–4693.
[4] J. Gaubicher, C. Wurm, G. Goward, C. Masquelier, L. Nazar, Chem. Mater. 12 (2000) 3240–3242.
[5] M. Sato, H. Ohkawa, K. Yoshida, M. Saito, K. Uematsu, K. Toda, Solid State Ionics 135 (2000) 137–142.
[6] S. Patoux, C. Wurm, M. Morcrette, G. Rousse, C. Masquelier, J. Power Sources 119–121 (2003) 278–284.
[7] J. Barker, M.Y. Saidi, US Patent 6,203,946 (2001).
[8] H. Huang, S.C. Yin, T. Kerr, N. Taylor, L.F. Nazar, Adv. Mater. 14 (2002) 1525–1528.
[9] S.C. Yin, P.S. Strobel, H. Grondey, L.F. Nazar, Chem. Mater. 16 (2004) 1456–1465.
[10] S.C. Yin, H. Grondey, P. Strobel, H. Huang, L.F. Nazar, J. Am. Chem. Soc. 125 (2003) 10402–10411.
[11] M.Y. Saidi, J. Barker, H. Huang, J.L. Swoyer, G. Adamson, J. Power Sources 119–121 (2003) 266–272.
[12] M.Y. Saidi, J. Barker, H. Huang, J.L. Swoyer, G. Adamson, Electrochem. Solid State Lett. 5 (2002) A149–A151.
[13] H. Huang, S.C. Yin, T. Kerr, N. Taylor, L.F. Nazar, Adv. Mater. 14 (21) (2002) 1525–1528.
[14] J. Barker, M.Y. Saidi, R.K.B. Gover, P. Burns, A. Bryan, J. Power Sources 174 (2007) 927–931.
[15] L.J. Fu, H. Liu, C. Li, Y.P. Wu, E. Rahm, R. Holze, Prog. Mater. Sci. 50 (2005) 881–928.
[16] M. Morcrette, J.B. Leriche, S. Patoux, C. Wurm, C. Masquelier, Electrochem. Solid State Lett. 6 (2003) A80–A84.
[17] M.M. Ren, Z. Zhou, Y.Z. Li, X.P. Gao, J. Yan, J. Power Sources 162 (2006) 1357–1362.
[18] D. Morgan, G. Ceder, M.Y. Saidi, J. Barker, J.L. Swoyer, H. Huang, G. Adamson, J. Power Sources 119–121 (2003) 755–759.
[19] P. Fu, Y.M. Zhao, Y.Z. Dong, X.N. An, G.P. Shen, Electrochim. Acta 52 (2006) 1003–1008.
[20] P. Fu, Y.M. Zhao, Y.Z. Dong, X.N. An, G.P. Shen, J. Power Sources 162 (2006) 651–657.
[21] C.M. Burba, R. Frech, Solid State Ionics 177 (2007) 3445–3454.
[22] Y.Z. Li, Z. Zhou, M.M. Ren, X.P. Gao, J. Yan, Electrochim. Acta 51 (2006) 6498–6502.
[23] Y.Z. Li, Z. Zhou, M.M. Ren, X.P. Gao, J. Yan, Mater. Lett. 61 (2007) 4562–4564.
[24] Y.Z. Li, Z. Zhou, X.P. Gao, J. Yan, Electrochim. Acta 52 (2007) 4922–4926.
[25] S.K. Zhong, Z.L. Yin, Z.X. Wang, H.J. Guo, X.H. Li, Trans. Nonferrous Met. Soc. China 16 (2006) S708–S710.
[26] X.J. Zhu, Y.X. Liu, L.M. Geng, L.B. Chen, J. Power Sources 184 (2008) 578–582.
[27] Q.Q. Chen, J.M. Wang, Z. Tang, W.C. He, H.B. Shao, J.Q. Zhang, Electrochim. Acta 52 (2007) 5251–5257.
[28] A.P. Tang, X.Y. Wang, Z.M. Liu, Mater. Lett. 62 (2008) 1646–1648.
[29] X.C. Zhou, Y.M. Liu, Y.L. Guo, Solid State Commun. 146 (2008) 261–264.
[30] S.K. Zhong, L.T. Liu, J.Q. Jiang, Y.W. Li, J. Wang, J.Q. Liu, Y.H. Li, J. Rare Earths 27 (2009) 134–137.